SLAC–PUB–6048
January 1993
T

Dependence on Dielectric Model and pH in a Synthetic Helical Peptide Studied by Monte Carlo Simulated Annealing*

YUKO OKAMOTO†

Stanford Linear Accelerator Center
Stanford University, Stanford, California 94309

Submitted to *Biopolymers*

* Work supported by the Department of Energy, contract DE–AC03–76SF00515.
† On leave of absence from Department of Physics, Nara Women's University, Nara 630, Japan.

ABSTRACT

Monte Carlo simulated annealing is applied to the tertiary structure prediction of a 17-residue synthetic peptide, which is known by experiment to exhibit high helical content at low pH. Two dielectric models are considered: sigmoidal distance-dependent dielectric function and a constant dielectric function ($\epsilon = 2$). Starting from completely random initial conformations, our simulations for both dielectric models at low pH gave many helical conformations. The obtained low-energy conformations are compared with the NOESY cross peak data for both main chain and side chains, and it is shown that the results for the sigmoidal dielectric function agree with the experimental data more than for the constant dielectric function. The failure of the constant dielectric function is interpreted to be due to the insufficiently screened repulsive electrostatic interactions among four positively charged residues at low pH. The results of the sigmoidal dielectric function predict the existence of two disjoint helices around residues 5–9 and 11–16. Simulations with high pH, on the other hand, hardly gave a helical conformation, which is also in accord with the experiment. Our results are compared with the previous molecular dynamics simulations of the same peptide.

INTRODUCTION

The discovery of significant α-helix formation of the C-peptide and S-peptide of RNase A in aqueous solution near 0° C[1–3] has changed the prevailing dogma that secondary structure within small peptides is undetectable.[4] Since then much work has been carried out on various small peptides to further elucidate the unexpected helical stability and to measure the helix propensities of amino acids.[5–18]

In this article we study the α-helix folding in an oligopeptide by Monte Carlo simulated annealing.[19] The major problem in traditional protein simulations such as molecular dynamics and Monte Carlo at temperatures of experimental interest (around 0° C) lies in the fact that simulations strongly depend on the initial conditions and cannot reach thermal equilibrium within the presently available computer resources. This is caused because the potential energy surface of protein system is very complicated and has a huge number of local minima. Hence, most simulations start from a folded structure such as an ideal helical conformation, and unfolding of the conformation is studied.[20–27] Simulated annealing alleviates this difficulty of dependence on initial conditions. The method was applied to crystallographic refinement of protein structures.[28–30] Its application to *ab initio* prediction of peptide and protein conformations was also proposed.[31–33] It was then shown that *folding* of the α-helix from a completely random initial conformation is indeed possible for various polypeptides which are empirically expected to be helical.[34–39] Moreover, it was shown that properties of β-strands can also be analyzed by this method.[40]

In the present work we consider the 17-residue synthetic peptide which was recently studied by two-dimensional nmr and CD spectroscopy.[9] The experimental data suggest that residues between 5 and 14 of this peptide are significantly helical at 278 K for pH 2.0 and that the helical content significantly decreases for high pH. The peptide was also studied in detail by molecular dynamics simulations.[23] In this work three different dielectric models: a linear distance-dependent dielectric function ($\epsilon = r$), a modified form[41] of the sigmoidal distance-dependent

dielectric function;[42] and $\epsilon = 1$ with explicit water molecules. It was shown that simulations with the sigmoidal dielectric function and the model with explicit water molecules resulted in average distances consistent with the nmr experiments,[9] with the sigmoidal function best representing the data.[23]

The purpose of the present article is to compare this well-performing sigmoidal dielectric function with yet another function, $\epsilon = 2$, within the framework of Monte Carlo simulated annealing. The latter function has been used in our previous works with Monte Carlo simulated annealing.[32–40]

METHODS

Potential Energy Function and Dielectric Models

The semi-empirical potential energy function that we used is given by the sum of the electrostatic term, 12-6 Lennard-Jones term, hydrogen-bond term, and torsion term with their parameters adopted from ECEPP/2.[44–46] The computer code KONF90[35,36] was used for Monte Carlo simulated annealing (SA).

Two dielectric functions for the electrostatic term were used for SA simulations: $\epsilon = 2$ and a sigmoidal distance-dependent dielectric function.[23] The sigmoidal dielectric function we used is given by

$$\epsilon(r) = D - \frac{D-2}{2}\Big[(sr)^2 + 2sr + 2\Big]e^{-sr} ,$$

where r is the interatomic distance, D is the bulk solvent dielectric constant, and s is a constant. We used $D = 78$ to represent an aqueous system and $s = 0.3$ following Ref. 23. This dielectric function is essentially the one used in Ref. 23 with the exception that they used $\frac{D-1}{2}$ instead of $\frac{D-2}{2}$. We introduced this modification in order to have the limit $\epsilon(r) \rightarrow 2$, as $r \rightarrow 0$, instead of $\epsilon(r) \rightarrow 1$. The dielectric function varies smoothly from 2 to 78 as r increases, following closely an experimentally derived curve.[47]

Peptide Preparation and Charges of Residues

The amino acid sequence of the 17-residue peptide is ETGTKAELLAKYEATHK.[9] Since the charges at peptide termini are known to reduce helix content,[43,6] we removed them by taking a neutral NH_2– group at the N-terminus and a neutral –COOH group at the C-terminus.

The ionization states of the amino acids were chosen to represent the peptide in two pH regions: low pH (< pH 4) and high pH (> pH 8). The charged residues are then His^+ and Lys^+ for low pH and Glu^- and Lys^+ for high pH.

Computational Details

One SA run consists of successively updating all the dihedral angles in the backbone and sidechains 10^4 times with the initial temperatue of 1000 K and the final temperature of 278 K (the experimentally relevant temperature). The temperature was decreased exponentially.[35,36] The peptide-bond dihedral angles ω were fixed to 180° for simplicity. Starting from completely random initial conformations, we made 20 SA runs for each of the following cases: with the two dielectric models for low pH and with the constant dielectric function ($\epsilon = 2$) for high pH. The CPU time for one SA run was $\sim$ 17 minutes with the constant dielectric function and $\sim$ 25 minutes with the sigmoidal dielectric function on a 2 GFLOPS supercomputer.

RESULTS AND DISCUSSION

α-Helix Formation

We label each set of 20 obtained conformations by numbers in increasing order. The ECEPP energies of Conformations # 1 (the lowest-energy conformation), # 10, and # 20 (the highest-energy conformation) are, for instance, −117.2 kcal/mol, −88.9 kcal/mol, and −67.8 kcal/mol, respectively, for the case of the sigmoidal dielectric function.

In order to analyze the α-helix propensities, we adopt the same criterion for α-helix as that defined in Ref. 36; we consider that a residue is in the α-helix state when the dihedral angles (ϕ, ψ) fall in the range $(-60 \pm 45°, -50 \pm 45°)$ in the

dihedral space. The *helicity* n is then defined by the number of successive residues which are in the α-helix state. Note that $n = 3$ corresponds to roughly one turn of the α-helix . We consider a conformation as helical if it has a segment with helicity $n \geq 3$.

In Table I we summarize the helix formation of all the runs. The first entry is the number of helical conformations ($n \geq 3$) listed against helicity n, the second entry is the average helicity $< n >_H$ which is an average over only helical segments ($n \geq 3$), and the third entry is the average fraction of residues in the α-helix state, $\frac{<n>}{N}$ ($N = 17$). The most remarkable feature we see in Table I is that at high pH helical conformations are hardly observed (1 out of 20), while at low pH many helical conformations are formed (11 for $\epsilon = \text{sig}$ and 14 for $\epsilon = 2$). This is in agreement with the experimental data.[9] This kind of charge dependence on helix stability was previously observed in experiments on C-peptide[5,6] and was confirmed theoretically by Monte Carlo simulated annealing.[36] We remark that 500 ps molecular dynamics simulations with the same 17-residue synthetic peptide did not reproduce this decline in helix formation for high pH.[23] At low pH both dielectric models produce similar amount of α-helix . The longest α-helix for both cases has helicity $n = 8$, i.e., more than two turns of the helix. While the case with $\epsilon = 2$ produced more helical conformations than that with $\epsilon = \text{sig}$ (14 versus 11), average helix fraction $\frac{<n>}{N}$ and average helicity $< n >_H$ are larger in the case with $\epsilon = \text{sig}$.

In Figure 1 we show the percentage of α-helix state as a function of residue number. The experimental values are also added in the Figure.[9,23] As expected, the results for high pH are significantly lower than those for low pH. Our data for the two dielectric functions at low pH have a few common tendencies. First, there is a clear decline at residue Thr-4, which is consistent with the experiments[9] and the molecular dynamics simulations.[23]. Secondly, there is another decline at residues Ala-10, which was not observed in the molecular dynamics simulations.[23] Unfortunately, experimental data for this residue are not available. (See Figure 1.) However, there is an important difference between $\epsilon = \text{sig}$ and $\epsilon = 2$ cases: the

sigmoidal dielectric function predicts high helix content in residues 11–15, while the constant dielectric function predicts only residue 14 to be in the α-helix state. This difference can be seen more clearly in Table II where we list the distribution of helices by classifying the obtained helices into three characteristic helices: Helix A (residues 1–3), Helix B (residues 5–9), and Helix C (residues 11–17). A helix which lies in-between two characteristic helices is listed under both characteristic helices when more than one residue belong to both. From the Table we conclude that the sigmoidal dielectric function predicts the existence of two disjoint helices, around residues 5–9 and 11–16, while the constant dielectric function mainly predicts the existence of only one helix around residues 5–9. The experimental data suggest that residues between 5 and 14 are significantly helical.[9] Hence, the sigmoidal dielectric function is more consistent with experiments. One more thing we can read off from Table II is that in both dielectric models low-energy conformations are mostly helical. The six lowest-energy conformation for $\epsilon = \text{sig}$ (Conformations # 1 - # 6) and ten lowest-energy conformation (Conformations # 1 - # 10) for $\epsilon = 2$ are all helical. The energy difference between the global-energy-minimum conformation (# 1) and the lowest-energy non-helical conformations (# 7 and # 11 for $\epsilon = \text{sig}$ and $\epsilon = 2$, respectively) are significant: $\Delta E = 25.3$ kcal/mol and 15.1 kcal/mol for $\epsilon = \text{sig}$ and $\epsilon = 2$, respectively (data not shown).

Comparison to 2D NMR Data

We now compare the tertiary structure predicted by the present simulations to the imlications of the NOESY connectivity data for both main-chain and side-chain pairs of atoms.[9] In Table III we summarize the distances corresponding to the observed NOESY connectivities for the three lowest-energy conformations (Conformation # 1 - # 3). When there are more than one possible interactions to consider, the shorter distance for each pair is taken. Here, we assumed that any distance ≤ 5 Åis consistent with the nmr data.[9] For the case of the sigmoidal dielectric function, Conformation #2 gave the most number of agreement (13 out of 21). For the case of the constant dielectric function, however, the three confor-

mations did not represent the structure closest to the experimental data. Instead Conformation # 12 gave the most number of agreement (10 out of 21), and the results of this conformation are also listed in the Table. As is clear from the Table, all of the three conformations from the sigmoidal dielectric function give reasonable agreement with the experiments, while the agreement is much poorer for the conformations for the constant dielectric function. In particular, the results for Conformation # 1 and # 2 for ϵ = sig imply the connectivity between Tyr-12 and His-16. The importance of this interaction for helix stability was noted by the molecular dynamics simulations[23] and the experiments.[9] In fact, a similar helix-stabilizing interaction betweem another aromatic residue Phe and His was previously noted in experiments.[7,8] This interaction can be interpreted to be a H-bond between the charged His side chain and the aromatic ring of Phe.[48,49] The importance of this Phe_i–His_{i+4} interactions for helix stability was further elucidated by a recent experiment.[50]

The root-mean-square distances (RMS) of these conformations in Table III were calculated (data not shown), and it was found that Conformations # 1 and # 2 are relatively similar to each other (RMS= 2.7 Åand 4.1 Åfor backbone atoms and all atoms, respectively) for ϵ = sig, while # 1 and # 12 are similar to each other (RMS= 2.6 Åand 3.6 Åfor backbone atoms and all atoms, respectively). Since Conformation # 12 gives the most number of agreement for $\epsilon = 2$, it can be said that the low energy conformations predicted by SA did not completely fail in reproducing the experimental data even in the case of the constant dielectric function.

End-to-End Distances

In Table IV we list the average end-to-end distances of the observed conformations for the three cases studied. The distance was measured from N of residue 1 to O of residue 17. The conspicuous feature observed in this Table is that $< d >$ for $\epsilon = 2$ at low pH is much larger than those for ϵ = sig at low pH and $\epsilon = 2$ at high pH. This fact can be interpreted as follows. Since there are four positive

residues at positions Lys-5^+, Lys-11^+, His-16^+, and Lys-17^+, and the rest of the residues are neutral at low pH, the electrostatic repulsions between like charges tend to stretch out the peptide. The constant dielectric function ($\epsilon = 2$) cannot screen this repulsive forces adequately, while the sigmoidal dielectric function which increases with distance can properly, resulting in more agreement with the experiments. On the other hand at high pH, charges are distributed at Glu-1^-, Lys-5^+, Glu-7^-, Lys-11^+, Glu-13^-, and Lys-17^+ with both positive and negative polarity. Hence, the problem of too much repulsion between like charges does not exist at high pH, and again an agreement with experiments (no helix formation) was obtained.

CONCLUSIONS

In this article we have applied Monte Carlo simulated annealing to the tertiary structure prediction of a 17-residue synthetic peptide. The most outstanding feature of the present method is that direct *folding* of helices is simulated from completely random initial conformations without any bias towards a helical conformation. We have compared the performance of two dielectric functions: the sigmoidal distance-dependent dielectric function[42,41,23] and the constant dielectric function ($\epsilon = 2$). Although both models reproduced about the same helical content, we have concluded that the former ($\epsilon = \mathrm{sig}$) is superior to the latter in the following points.

(1) Location of helices are more in agreement with the experiments.[9] Two disjoint helices were predicted around residues 5–9 and 11–16, while the experimental data suggest that residues between 5 and 14 are significantly helical.

(2) NOESY connectivity data for both main chain and side chains agree more with the experiments.[9] In particular, the interaction between Tyr-12 and His-16^+ was observed in accord with the molecular dynamics simulations[23] and the experiments.[9]

The failure of the constant dielectric model was interpreted to be due to the

insufficient screening of the strong electrostatic repulsions among the four positive residues. We have also confirmed the experimental data suggesting notable decline in helix content at high pH, which was not observed by the previous molecular dynamics simulations.[23]

Although a simulation with explicit water molecules should eventually be performed, they are substantially more computer intensive (factor of 30 for the 17-residue synthetic peptide) and are also slower in the thermalization process (sampling smaller conformational space) than the one with the sigmoidal dielectric function.[23] Considering the successes in *ab initio* prediction of tertiary structure in the present work, we draw the same conclusion as the previous molecular dynamics simulations: within the presently available computer resources, the sigmoidal dielectric function is an attractive alternative to adding explicit water molecules.

Acknowledgements:

The auther would like to thank Professor R.L. Baldwin and Dr. V. Daggett of Stanford University School of Medicine for many helpful discussions and suggestions. He is also grateful to the members of Baldwin Group and Stanford Linear Accelerator Center for their kind hospitality.

REFERENCES

1. Brown, J.E. & Klee, W.A. (1971) *Biochemistry* **10**, 470–476.
2. Bierzynski, A., Kim, P.S. & Baldwin, R.L. (1982) *Proc. Natl. Acad. Sci. USA* **79**, 2470–2474.
3. Kim, P.S. & Baldwin, R.L. (1984) *Nature* **307**, 329–334.
4. Epand, R.M. & Scheraga, H.A. (1968) *Biochemistry* **7**, 2864–2872.
5. Shoemaker, K.R., Kim, P.S., Brems, D.N., Marqusee, S., York, E.J., Chaiken, I.M., Stewart, J.M. & Baldwin, R.L. (1985) *Proc. Natl. Aca. Sci. USA* **82**, 2349–2353.
6. Shoemaker, K.R., Kim, P.S., York, E.J., Stewart, J.M. & Baldwin, R.L. (1987) *Nature* **326**, 563–567.
7. Dadlez, M., Bierzynski, A., Godzik, A., Sobocinska, M. & Kupryszewski, G. (1988) *Biophys. Chem.* **31**, 175–181.
8. Shoemaker, K.R., Fairman, R., Schultz, D.A., York, E.J., Steward, J.M. & Baldwin, R.L. (1990) *Biopolymers* **29**, 1–11.
9. Bradley, E.K., Thomason, J.F., Cohen, F.E. & Kuntz, I.D. (1990) *J. Mol. Biol.* **215**, 607–622.
10. Padamanabhan, S., Marqusee, S., Ridgeway, T., Laue, T.M. & Baldwin, R.L. (1990) *Nature* **344**, 268–270.
11. Merutka, G., Lipton, W., Shalango, W., Park, S.-H. & Stellwagen, E. (1990) *Biochemistry* **29**, 7511–7515.
12. O'Neil, K.T. & DeGrado, W.F. (1990) *Science* **250**, 646–651.
13. Lyu, P.C., Liff, M.I., Marky, L.A. & Kallenbach, N.R. (1990) *Science* **250**, 669–673.
14. Chakrabartty, A., Schellman, J.A. & Baldwin, R.L. (1991) *Nature* **351**, 586–588.

15. Gans, P.J., Lyu, P.C., Manning, M.C., Woody, R.W. & Kallenback, N.R. (1991) *Biopolymers* **31**, 1605–1614.

16. Kemp, D.S., Boyd, J.G. & Muendel, C.C. (1991) *Nature* **352**, 451–454.

17. Stellwagen, E., Park, S.-H., Shalango, W. & Jain, A. (1992) *Biopolymers* **32**, 1193–1200.

18. Chakrabartty, A. & Baldwin, R.L. (1992) in *Protein Folding: In Vivo and In Vitro*, Cleland, J. & King, J., Eds., ACS Press, in press.

19. Kirkpatrick, S., Gelatt, C.D., Jr. & Vecchi, M.P. (1983) *Science* **220**, 671–680.

20. Levy, R.M., Perahia, D. & Karplus, M. (1982) *Proc. Natl. Acad. Sci. USA* **79**, 1346–1350.

21. Brooks, B.R. (1989) *Chem. Scripta* **29A**, 165–169.

22. Tirado-Rives, J. & Jorgensen, W.L. (1991) *Biochemistry* **30**, 3864–3871.

23. Daggett, V., Kollman, P.A. & Kuntz, I.D. (1991) *Biopolymers* **31**, 285–304.

24. Daggett, V., Kollman, P.A. & Kuntz, I.D. (1991) *Biopolymers* **31**, 1115–1134.

25. Soman, K.V., Karimi, A. & Case, D.A. (1991) *Biopolymers* **31**, 1351–1361.

26. Hermans, J., Anderson, A.G. & Yun, R.H. (1992) *Biochemistry* **31**, 5646–5653.

27. Daggett, V. & Levitt, M. (1992) *J. Mol. Biol.* **223**, 1121–1138.

28. Nilges, M., Clore, G.M. & Gronenborn, A.M. (1988) *FEBS Lett.* **229**, 317–324.

29. Brünger, A.T. (1988) *J. Mol. Biol.* **203**, 803–816.

30. Brünger, A.T., Karplus, M. & Petsko, G.A. (1989) *Acta Cryst.* A**45**, 50–61.

31. Wilson, S.R., Cui, W., Moskowitz, J.W. & Schmidt, K.E. (1988) *Tetrahedron Lett.* **29**, 4373–4376.

32. Kawai, H., Kikuchi, T. & Okamoto, Y. (1989) *Protein Eng.* **3**, 85–94.

33. Wilson, C. & Doniach, S. (1989) *Proteins* **6**, 193–209.

34. Wilson, S.R. & Cui, W. (1990) *Biopolymers* **29**, 225–235.

35. Kawai, H., Okamoto, Y., Fukugita, M., Nakazawa, T. & Kikuchi, T. (1991) *Chem. Lett.* **1991**, 213–216.

36. Okamoto, Y., Fukugita, M., Nakazawa, T. & Kawai, H. (1991) *Protein Eng.* **4**, 639–647.

37. Fukugita, M., Nakazawa, T., Kawai, H. & Okamoto, Y. (1991) *Chem. Lett.* **1991**, 1279–1282.

38. Okamoto, Y., Kikuchi, T., Nakazawa, T. & Kawai, H. (1992) "Prediction of Tertiary Structure of Parathyroid Hormone Fragment (1-34) by Monte Carlo Simulated Annealing", Nara Women's University preprint NWU-7/92, submitted for publication.

39. Okamoto, Y. (1993) "α-Helix Propensities of Nonpolar Amino Acids Predicted by Monte Carlo Simulated Annealing", SLAC-PUB-6043, submitted for publication.

40. Nakazawa, T., Kawai, H., Okamoto, Y. & Fukugita, M. (1992) *Protein Eng.* **5**, 495–503.

41. Ramstein, J. & Lavery, R. (1988) *Proc. Natl. Acad. Sci. USA* **85**, 7231–7235.

42. Hingerty, B.E., Ritchie, R.H., Ferrell, T.L. & Turner, J.E. (1985) *Biopolymers* **24**, 427–439.

43. Ihara, S., Ooi, T. & Takahashi, S. (1982) *Biopolymers* **21**, 131–145.

44. Momany, F.A., McGuire, R.F., Burgess, A.W. & Scheraga, H.A. (1975) *J. Phys. Chem.* **79**, 2361–2381..

45. Némethy, G., Pottle, M.S. & Scheraga, H.A. (1983) *J. Phys. Chem.* **87**, 1883–1887.

46. Sippl, M.J., Némethy, G. & Scheraga, H.A. (1984) *J. Phys. Chem.* **88**, 6231–6233.

47. Conway, B.E., Bockris, J.O. & Ammar, I.A. (1951) *Trans. Faraday Soc.* **47**, 756–766.

48. Burley, S.K. & Petsko, G.A. (1986) *FEBS Lett.* **203**, 139–143.

49. Levitt, M. & Perutz, M.F. (1988) *J. Mol. Biol.* **201**, 751–754.

50. Armstrong, K.M., Fairman, R. & Baldwin, R.L. (1992) "The (i,i+4) Phe-His Interaction Studied in an Alanine-based α-Helix", to be published.

Table I. α-Helix Formation in 20 Monte Carlo Simulated Annealing Runs[a]

pH[b]	Low	Low	High
Dielectric Model[c]	$\epsilon = \text{sig}$	$\epsilon = 2$	$\epsilon = 2$
n			
3	3	4	1
4	2	4	0
5	3	3	0
6	1	2	0
7	1	0	0
8	1	1	0
9	0	0	0
10	0	0	0
Total	11/20	14/20	1/20
$< n >_H$	4.4	4.2	3.0
$\frac{<n>}{N}$	0.44	0.41	0.11

[a] The number of helical conformations (i.e., conformations with helicity $n \geq 3$) for each n is listed. Entries with $n > 10$ are suppressed, since they are all null entry. Average helix length $< n >_H$ and average fraction of residues in the α-helix state $\frac{<n>}{N}$ are also listed.

[b] Low pH and high pH are defined by the conditions pH < pH 4 and pH > pH 8, respectively.

[c] The $\epsilon = \text{sig}$ refers to the sigmoidal distance-dependent dielectric function.

Table II. Distribution of Helices at Low pH[a]

ϵ = sig				ϵ = 2			
Conf.	Helix A	Helix B	Helix C	Conf.	Helix A	Helix B	Helix C
1		5–9	11–15	1		7–11	
2	2–9	2–9	11–15	2	2–4		
3		5–11	14–16	3			12–14
4	2–5		11–15	4		5–9	12–14
5			11–16	5	1–6	1–6	
6		7–9		6	2–9	2–9	12–14
9			12–15	7		6–9	
10		4–6	12–15	8		7–9	
11	1–3	7–9	11–13	9		6–9	
16		5–7		10		6–9	
20		4–8		12		6–11	
				13		5–7	10–14
				16	1–3		
				18		6–9	
Total	3/11	8/11	8/11	Total	4/14	11/14	4/14

[a] Helix A is defined to be a helix in residues 1–3, Helix B in 5–9, and Helix C in 11–17. When a helix lies in one of the three characteristic helices for more than one residue, it is counted and listed (i.e., edge residues are not counted; a helix in residues 2–6 is counted as both Helix A and Helix B, but a helix in resiudes 2–5 is counted as only Helix A).

Table III. Distances (in Å) Corresponding to Observed NOESY Cross Peaks for the Three Lowest-Energy Conformations from 20 Monte Carlo Simulated Annealing Runs[a]

Dielectric Model	sig	sig	sig	2	2	2	2
Conformation	1	2	3	1	2	3	12
E (kcal/mol)	−117.2	−102.2	−99.3	26.1	31.1	31.2	41.2
Helix 1	5–9	2–9	5–11	7–11	2–4	12–14	6–11
Helix 2	11–15	11–15	14–16				
Main Chain							
$\alpha_4\eta_6$	3.2	4.2	3.2	4.4	4.9	4.4	3.3
$\alpha_5\eta_8$	3.0	3.0	2.8	7.3	8.0	8.4	3.1
$\alpha_5\beta_8$	2.3	2.6	2.2	9.2	8.0	10.4	3.2
$\alpha_6\beta_9$	2.9	2.9	3.2	5.0	9.1	9.1	2.7
$\alpha_8\beta_{11}$	7.0	6.2	2.9	3.1	7.7	7.7	2.9
$\alpha_{10}\eta_{13}$	4.3	3.8	5.3	4.8	6.7	4.1	4.9
$\alpha_{11}\eta_{14}$	3.1	3.2	8.9	8.4	8.4	4.1	8.8
$\alpha_{13}\eta_{16}$	4.1	3.2	4.4	7.1	6.9	5.3	7.1
Coincidence	7/8	7/8	6/8	4/8	1/8	3/8	6/8
Side Chain							
$\beta_4\eta_6$	3.7	5.4	3.7	4.0	3.9	4.5	3.0
$\eta_5\gamma_8$	7.5	5.5	7.6	11.2	9.9	13.0	6.7
$\alpha_5\delta_8$	3.4	2.3	3.5	11.1	9.2	11.6	2.7
$\eta_5\delta_8$	6.0	4.6	5.9	11.3	8.0	12.0	5.5
$\alpha_5\gamma_8$	4.8	3.5	4.7	11.6	10.7	12.1	3.9
$\delta_9\beta_{12}$	10.7	7.0	5.0	4.2	8.7	10.8	4.1
$\delta_9\epsilon_{12}$	13.5	11.1	9.4	8.4	12.8	15.3	7.8
$\delta_9\delta_{12}$	11.4	8.7	6.9	5.9	10.4	12.8	5.3
$\delta_9\gamma_{13}$	8.2	9.3	3.9	5.1	12.7	11.5	5.9
$\gamma_9\gamma_{13}$	9.3	11.4	3.8	4.7	11.5	11.5	8.4
$\delta_{12}\epsilon_{16}$	6.5	3.4	8.5	8.3	6.7	8.6	10.9
$\epsilon_{12}\beta_{16}$	3.7	3.6	5.5	13.1	6.4	3.7	13.9
$\epsilon_{12}\epsilon_{16}$	4.2	3.0	10.3	10.7	4.5	8.8	13.2
Coincidence	5/13	6/13	6/13	3/13	2/13	2/13	4/13
Total Coincidence	12/21	13/21	12/21	7/21	3/21	5/21	10/21

[a] Coincidence is defined to be any distance $\leq$ 5 Å. For $\epsilon = 2$ the results for the twelfth lowest-energy conformation are also listed for comparison, since they give the most number of coincidence with the experimental data within this dielectric model. The ranges of residue numbers in the α-helix state are listed in the Helix entry. Relatvie energy differences between the two dielectric models are meaningless.

Table IV. End-to-End Distance (in Å)[a]

Dielectric Model	pH	$< d >$	σ
$\epsilon =$ sig	Low	12.4	5.1
$\epsilon = 2$	Low	27.6	5.1
$\epsilon = 2$	High	9.6	3.1

[a] End-to-end distance is measured from N of residue 1 to O of residue 17. $< d >$ is the average end-to-end distance and σ is the corresponding standard deviation.

FIGURE CAPTIONS

1) Percentage of helix as a function of residue number. Open squares are the experimental values from ratios of intensities of main-chain NOESY cross peaks at pH 2.[9] Values from Monte Carlo simulated annealing are the results of 20 runs with ϵ = sig (connected solid squares) for low pH, $\epsilon = 2$ (connected solid triangles) for low pH, and $\epsilon = 2$ (connected solid circles) for high pH.

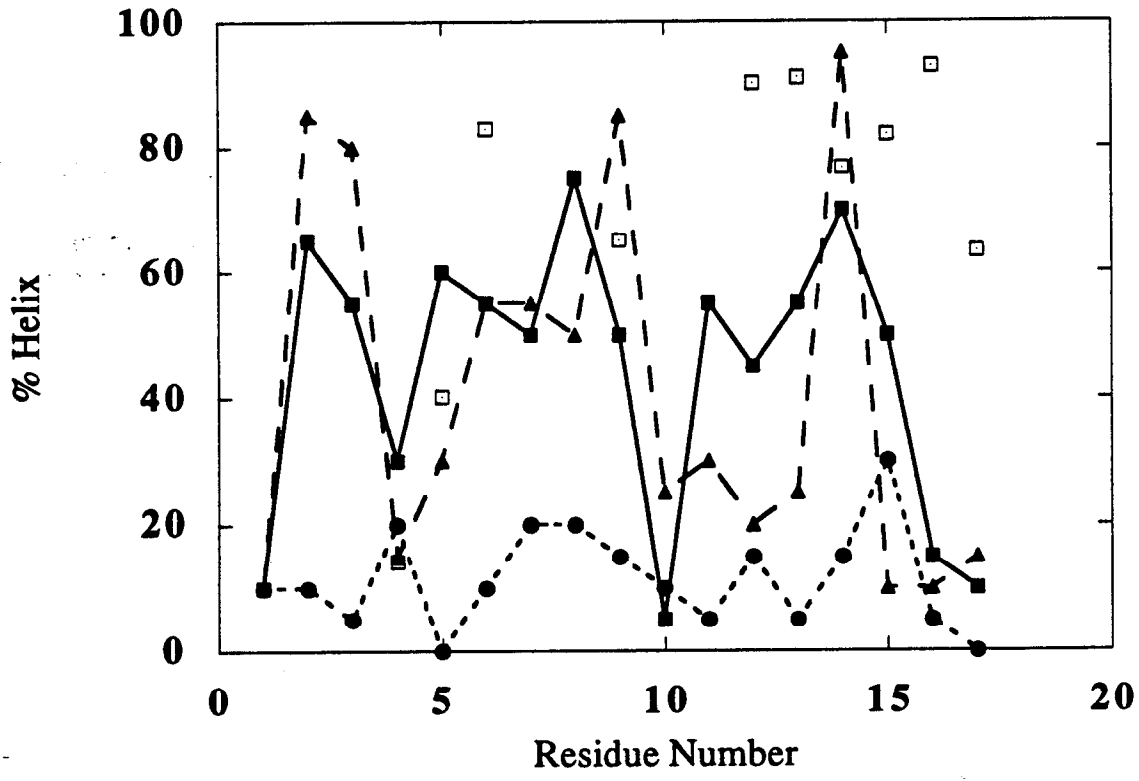

Fig. 1